RESEARCH ARTICLE

BON VIEW PUBLISHING

High-Temperature Sensing with Iron-Ceramic Enhanced Fiber Bragg Grating Sensors: Encapsulation Strategies and Concentration Dependencies

Raja Yasir Mehmood Khan[1], Rahim Ullah[1] and Muhammad Faisal[1],*

[1]*National Institute of Lasers and Optronics College, Pakistan Institute of Engineering and Applied Sciences, Pakistan*

Abstract: This research article primarily aims to enable type-I FBG(fiber Bragg grating) for high-temperature sensing and to explore the influence of varying concentrations of iron fillings in the ceramic on the sensor's sensitivity and response time. A set of six identical probes were fabricated, each with a different iron filling concentration ranging from 0% to 50%. Increasing the iron filling concentration from 0% to 50% enhanced the temperature sensitivity of the probe from 14.08 ± 0.24 pm/°C to 14.67 ± 0.17 pm/°C. To evaluate the response time, the probes were subjected to an abrupt heating process from 27 °C to 700 °C, and the duration was measured. The response time improved from 270 s to 180 s, representing a 33.33% improvement, as the iron filling concentration increased from 0% to 50%. Beyond a 40% concentration, both the temperature sensitivity and response time reached saturation. The lifetime of the optimized probe with a 40% iron filling concentration is estimated to be 4.46 years. During repeated exposures to high temperatures, no permanent drift in its Bragg wavelength was observed, and its repeatability during a heating-cooling cycle exhibited hysteresis of less than 1%.

Keywords: type-I FBG(fiber Bragg grating), temperature sensitivity, temporal response, iron fillings, wavelength drift

1. Introduction

Since the discovery of fiber Bragg gratings (FBGs) by K. Hill in 1978, extensive research has been conducted on their applications in temperature and strain sensing. FBGs have been successfully utilized to develop temperature sensors for various environments, including cryogenic, high-temperature, and ultra-high-temperature environments [1–5]. With the increasing demand for high-temperature sensors in fields such as nuclear reactors, aerospace, combustors, and turbines, significant efforts have been dedicated to exploring the high-temperature sensing capabilities of FBGs over the past a few decades [6–9].

Type-I FBGs are typically manufactured through the partial modulation of the refractive index in the core of an optical fiber. This modulation is achieved either by exposing a photosensitive optical fiber to UV or femtosecond (fs) laser beams using a phase mask technique or by directly inscribing a non-photosensitive optical fiber point-by-point with fs-lasers [10–12]. These standard type-I FBGs are commonly stabilized to meet the specifications required for telecommunications. This includes ensuring they can operate within a temperature range of −20 °C to 80 °C with lifespan of approximately 25 years [13]. However, these gratings exhibit thermal degradation when exposed to high temperatures, leading to the breakage of Si-Si, Si-Ge, Ge-Ge, Si-O, and Ge-O

bonds [14]. As a consequence, standard type-I FBGs are limited to temperature sensing below 200 °C. To enable the FBG sensors in high-temperature applications, several mechanisms have been introduced, including FBG regeneration, metallic coating, and encapsulation of FBGs. These strategies aim to mitigate thermal degradation and enhance the sensor's robustness and longevity in challenging temperature environments [15–17].

The technique of regeneration involves subjecting seed gratings to high-temperature processing at temperatures ranging from 700 °C to 900 °C. This process completely erases the existing gratings and leads to the formation of new thermally stable gratings in the regions exposed to a UV laser. These regenerated FBGs (RFBGs) have garnered significant attention for their potential in high and ultra-high-temperature sensing applications [18]. Bian et al. [19] demonstrated the production of RFBG in large mode area optical fibers, enabling temperature sensing of the FBG up to 800 °C. Similarly, Yu et al. [20] reported the creation of RFBG in hydrogen-loaded optical fiber, achieving high-temperature sensing up to 800 °C with a temperature sensitivity of 12 pm/°C. Wang et al. [21] employed a post-annealing process to produce RFBG, enabling ultra-high-temperature sensing up to 1295 °C with a temperature sensitivity of 16 pm/°C. However, the lifetime of their sensor was limited to only 10 min. In another study, Sato et al. [22] examined the effects of thermal aging on RFBGs at temperatures surpassing their regeneration temperature. Their findings revealed that the lifespan of RFBGs is merely a few hours when exposed to temperatures exceeding their regeneration

***Corresponding author:** Muhammad Faisal, National Institute of Lasers and Optronics College, Pakistan Institute of Engineering and Applied Sciences, Pakistan. Email: mfaisal13@yahoo.com

temperature. Ceramic and metallic encapsulated RFBGs have also been explored in the literature, allowing for high and ultra-high-temperature sensing. These encapsulated RFBGs exhibited temperature sensitivities ranging from 9.5 pm/°C to 16 pm/°C, with lifetimes varying from a few hours to a few years [14, 23]. Although RFBGs have enabled the sensing of high and ultra-high temperatures, they have certain drawbacks. These include weaker mechanical strength due to the burning of the protective coating during high-temperature processing, brittleness of the glass, lower grating strength (10^{-3} gratings), and reduced reflectivity (<30%) [24–26]. The weaker grating strength poses challenges for achieving apodization in RFBGs.

The technique of metallic coating involves direct application of metals such as gold, silver, nickel, and copper onto FBGs. Wang et al. [27] achieved high-temperature sensing up to 800 °C by metallic coatings of the FBGs. He et al. [28] synthesized a molybdenum-copper coated FBG, enabling high-temperature sensing up to 800 °C with a temperature sensitivity of 15.27 pm/°C. However, the lifetime of their coated FBG was limited to less than 1 hour. Different methods such as electroplating, chemical and physical vapor deposition, chemical sputtering, and thermal spraying are employed for the metallic coating of FBGs. Metallic coating provides an alternative approach, alongside regeneration, for utilizing FBGs in high-temperature sensing. However, metallic coatings have certain drawbacks. They tend to have limited durability, and the high temperatures encountered can induce thermal shocks within the metallic structure, potentially leading to the fracture of the coated FBGs. Moreover, due to direct contact, metallic coatings impose thermal stresses on FBGs, necessitating thorough stress analysis in such cases [29]. Additionally, metallic coating can be costly in terms of the required equipment and materials. Optical fibers, composed of insulating material (such as silica) and having micron-scale diameters, present challenges for achieving a uniform metallic coating.

Compared to regenerating a seed FBG and applying a metallic coating, encapsulating an FBG offers a straightforward, cost-effective solution that maintains the desirable characteristics of a standard FBG, such as mechanical strength, grating strength, high reflectivity (> 90%), and easy apodization. Encapsulation of an FBG can be achieved using commonly available materials like stainless steel (SS), copper, Inconel, etc. In an encapsulation, optical fiber is kept free from one end which immunes the encapsulated FBGs from external stresses in the encapsulated structures. Given the fragile nature of an FBG, its application in harsh environments requires extra care and attention. However, encapsulation enhances the strength of an FBG, facilitating its convenient handling and enabling its application in challenging conditions.

Various types of encapsulations have been reported for type-I FBGs, enabling them to sense high and ultra-high temperatures. Kuncha et al. [30] employed an encapsulation method involving an Inconel tube, followed by a low thermal conductive ceramic tube, achieving ultra-high-temperature sensing in a boiler up to 1100°C. This design also incorporated the flow of water as a coolant through the encapsulated structure at a specific speed, making it complex and less sensitive to temperature gradients. Mamidi et al. [31] encapsulated FBGs in capillaries made of silicon carbide, boron silicate, SS, copper, and aluminum nitride, successfully achieving temperature sensing up to 500°C. Their optimized sensor exhibited a 25% decrease in reflected power when heated from 20°C to 500°C with sensitivity of 14.03 ± 0.02 pm/°C. Reddy et al. [32] created a sensor package capable of measuring ultra-high temperatures using a type-I FBG as the sensor. The sensor was constructed by affixing a type-I FBG onto two metallic strips made of SS and mild steel. It

was then enclosed within a rectangular frame made of SS. They were able to achieve ultra-high-temperature sensing up to 1000 °C with this setup. They accomplished this by taking advantage of the difference in thermal expansions between SS and mild steel, which induced a temperature-dependent strain on the FBG. As a result, the sensor exhibited a non-linear response with an incase in temperature. The plain concrete is susceptible to strength degradation and low thermal conductivity at elevated temperatures. Huang et al. [33] report that iron tailing powder (ITP), a waste material from iron workshops and steel mills, can enhance the performance of ultra-high-performance concrete when subjected to high temperatures. They claimed that the addition of ITP increases the number of micropores or cracks in concrete. Therefore, the concrete incorporating 15% ITP maintains 53.8% of its original strength at 800°C, unlike the concrete without ITP that maintains 31.6% of its original strength. Similarly, Dawood and Dawood et al. [34] investigated the strength properties of concrete produced by replacing sand with iron filings and found an increase in strength of the concrete as compared to the reference concrete. Jain and Sancheti [35] in their experimental investigation also found an increase in strength of concrete with addition of iron.

In this study, we explored the benefits of encapsulating FBG sensors and incorporating iron fillings into concrete ceramic to develop a temperature sensor probe based on type-I FBG encapsulation. The probe utilized a mixture of concrete ceramic as a filler material, with varying concentrations of iron fillings (ranging from 0% to 50%) added to enhance its properties. The concentration of iron fillings demonstrated a significant influence on the sensitivity and response time of the sensing probes. Additionally, we investigated the permanent wavelength drift or hysteresis of the probe through repeated exposure to high temperatures. This analysis is crucial for the practical application of the probe in prolonged high-temperature environments with potential temperature fluctuations. The resulting probe is cost-effective, easy to manufacture, and reinforces the strength of FBG sensors, facilitating robust and straightforward handling for high-temperature sensing applications in challenging conditions. To the best of our knowledge, no previous studies have reported on the impact of iron fillings in plain concrete ceramic on the temperature sensitivity and response time of FBG temperature sensors.

2. Experimental Methodology

In this experiment, we have fabricated six distinct temperature sensing probes, each possessing different concentration of iron fillings in the filler. To manufacture these probes, we first placed a 10 mm long FBG spliced with a single mode fiber into a SS capillary, which measures 25.5 cm in length, 1 mm in outer diameter, and 0.5 mm in internal diameter. One end of the FBG was intentionally left free within the capillary tube to avoid unwanted strain and enable smooth thermal expansion. The SS capillary is then inserted inside the center of another SS tube, which measures 24 cm in length, 6 mm in outer diameter, and 4 mm in inner diameter. The 15 mm end of the capillary was left out for external capping purposes. The SS tube is then uniformly filled with the ceramic paste blended with iron fillings followed by a 24-hour drying process at 60 °C. After drying, the free end of the SS capillary is capped with another SS tube measuring 4.5 cm in length, 12 mm outer diameter, 8 mm in inner diameter.

To make the sensing probes distinctive, both the SS tube end SS cap of each probe were filled with the paste blended with iron fillings, ranging from 0% to 50% followed by a 24-hour drying process. Subsequently, the probes underwent annealing at 200 °C for 1 hour

Figure 1
Schematic of the designed probes. Geometry of the designed probes is kept same while concentration of iron fillings varied from 0% to 50%
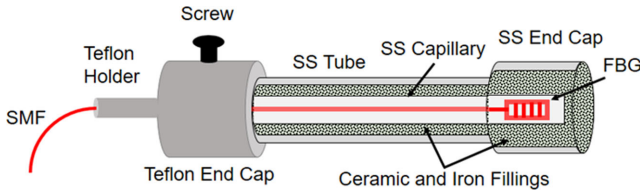
to eliminate residual water and stabilize the ceramic structure within them. After the annealing process, the probes were allowed to cool for two hours before being equipped with Teflon holders, ensuring convenient handling. Figure 1 displays a generic representation of the probe's schematic.

Experimental setup of the experiment consists of a broadband light source (BBS) (L band: 1530–1600 nm) (EXFO Electro Optical Engineering Inc.), an optical spectrum analyzer (OSA) (C+L band, 1250–1650 nm), (EXFO Electro Optical Engineering Inc.), a high-speed power meter (800–1700 nm) (InGaAs, EXFO Electro Optical Engineering Inc., Canada), a box furnace (maximum temperature range 1100 °C) (L51R, Nabertherm, Germany), an optical circulator (Shenzhen Optics, China), a general purpose interface bus (GPIB) and single mode optical fiber (SMF), six FBGs (Length = 10mm, Bandwidth ≤ 0.3 nm, Reflectivity 90%, Coating = polyimide). Schematic of the experimental setup is shown in Figure 2. BBS launches a broadband spectrum of light in the SMF which is directed towards the sensing probe with the help of the three-port circulator. The sensing probe reflects a particular wavelength termed as Bragg wavelength (λ_B). The λ_B is dependent to grating period (Λ) and effective refractive index (n_{eff}) of the FBG. Mathematically [3]:

$$\lambda_B = 2n_{eff}\Lambda \qquad (1)$$

Probes are inserted in the furnace one by one, and temperature is varied from 27 °C to 700 °C at the rate of 12 °C per minute, and respective change in λ_B is monitored by using the OSA interfaced with a laptop by using the GPIB. For each probe, the experiment is repeated three times and average shift in λ_B is calculated.

3. Results and Discussions

To assess the impact of encapsulation on the reflection spectra of encapsulated FBGs, firstly, Bragg spectrum of a bare FBG is recorded at 27 °C as shown in Figure 3(a). To ensure the stability of the FBGs encapsulated within the probes even at elevated temperatures (700 °C), Bragg spectra of the encapsulated FBGs in the developed probes were recorded and displayed in Figure 3(b). Remarkably, the Bragg spectra of all the probes were found to be identical to those of the bare FBG at 27 °C, providing clear evidence of their consistent and thermally stable performance under high-temperature conditions and chirping-free response after encapsulation further supports their stable behavior. The reason that a type-I FBG can sense high temperatures up to 700°C without vanishing when encapsulated in an iron-ceramic package lies in the thermal insulation provided by the encapsulation. The encapsulation package scales down the temperature that reaches the FBG, allowing heat to reach the FBG indirectly. This indirect heat transfer ensures that the FBG can sense high temperatures without compromising its thermal stability. While the chirping-free response is likely attributed to the freedom of the FBGs' ends within the internal capillaries of the probes, which effectively protect the FBGs from external stresses during the encapsulation process.

Firstly, a bare FBG was inserted into the furnace, and the shift in its λ_B was recorded over a temperature range from 27°C to 200°C, as illustrated in Figure 4(a). The bare FBG exhibited a linear red shift in its λ_B with increasing temperature. The temperature sensitivity of the bare FBG was determined to be 16.33 ± 0.13 pm/°C. Figure 4(b–g) illustrate the average shift in λ_B of FBGs encapsulated in the probes

Figure 2
Schematic representation of the experimental setup used for experimental analysis of the designed FBG temperature sensors
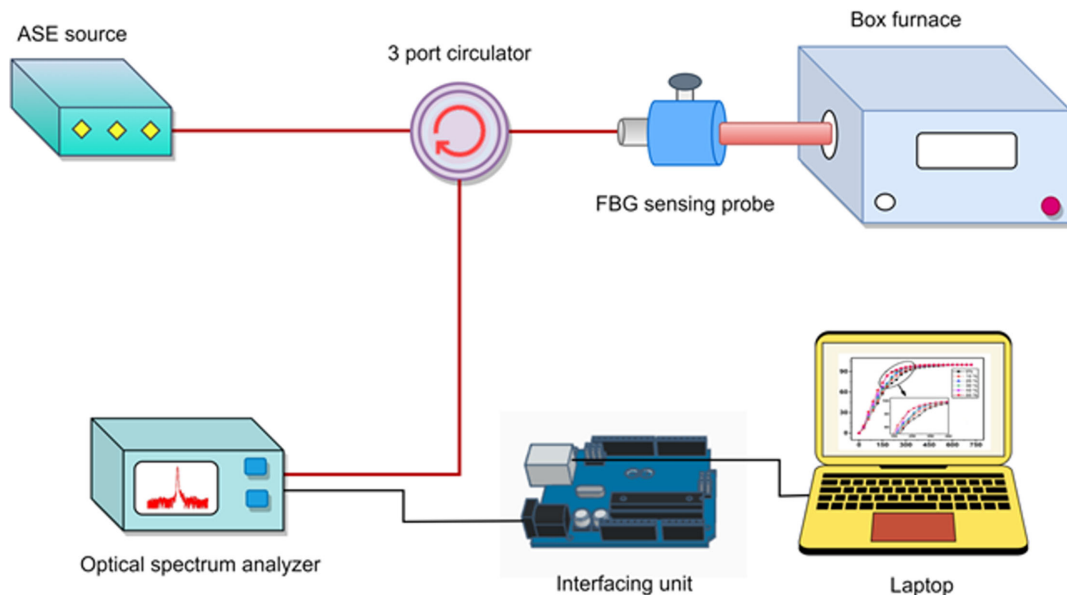
Figure 3
Reflection spectra of (a) bare FBG of Bragg wavelength of 1549.955 nm at 27°C and (b) FBGs encapsulated in the probes with 0% to 50% iron filling concentration at 700°C
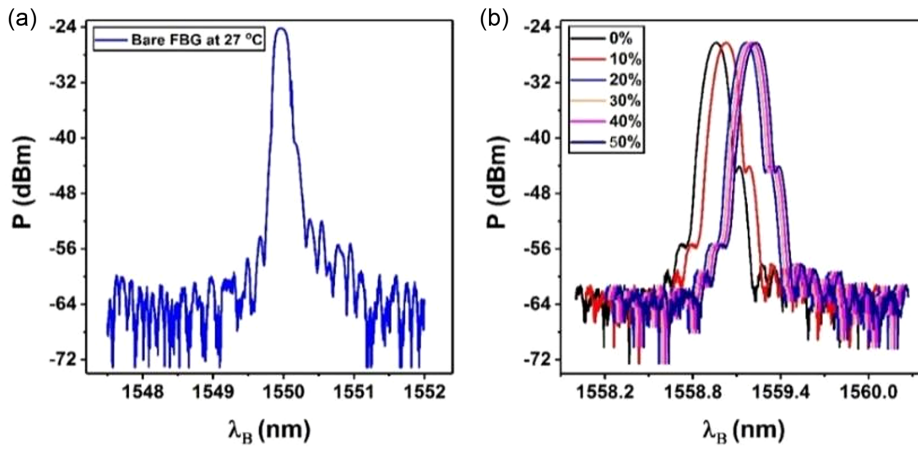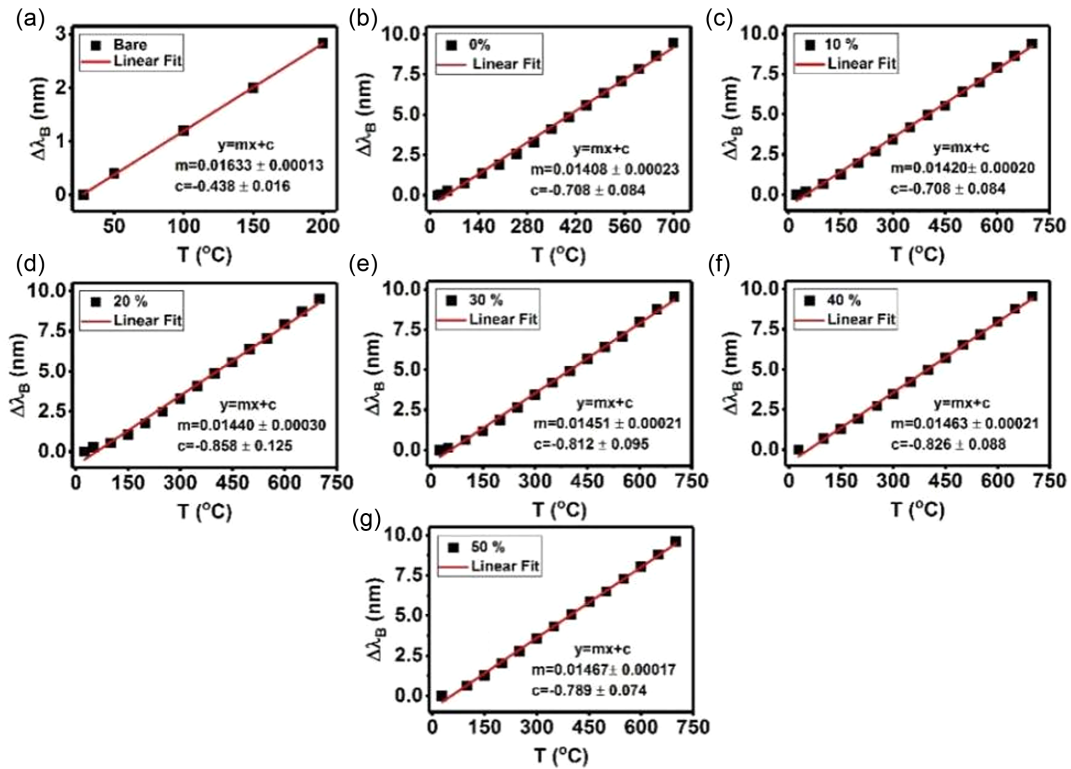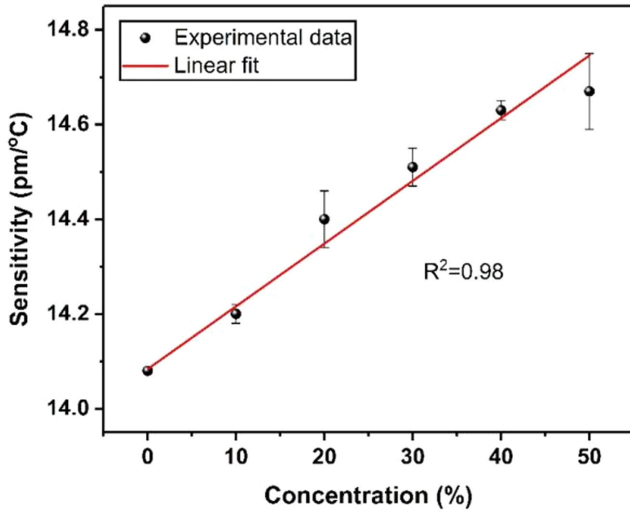

Figure 4
(a) Shift in Bragg wavelength of bare FBG with increase in temperature from 27°C to 200°C. (b–g) Shift in Bragg wavelength with increase in temperature from 27°C to 700°C of encapsulated FBGs in probes with iron fillings concentration (0%, 10%, 20%, 30%, 40%, and 50%), respectively. Solid lines represent linear fit to the experimental data

with varying iron filling concentrations (0%, 10%, 20%, 30%, 40%, and 50%), respectively as the temperature increases from 27 °C to 700 °C. A linear increasing trend is observed in the shift of λ_B, with a coefficient of regression exceeding 0.99, indicating excellent linearity in their responses. The temperature sensitivities of the probes, corresponding to the different iron filling concentrations, are as follows: 14.08 ± 0.24 pm/°C, 14.20 ± 0.20 pm/°C,

14.40 ± 0.30 pm/°C, 14.51 ± 0.21 pm/°C, 14.63 ± 0.21 pm/°C, and 14.67 ± 0.17 pm/°C. Compared to the bare FBG, all the probes were found to have lower sensitivities. Encapsulating an FBG reduces the amount of heat reaching the FBG, which results in lower sensitivity. However, this has a positive aspect: by reducing the heat reaching the FBG, the encapsulation allows the FBG to maintain thermal stability in high-temperature environments.

Figure 5
Variation in temperature sensitivity of FBGs encapsulated in the probes with an increase in concentration of iron fillings

Table 1
Temperature sensitivities and temporal responses of the sensors with iron fillings concentration varying from 0% to 50%

No.	Iron filling concentration (%)	Temperature sensitivity (pm/°C)	Temporal response (s)
1.	0	14.08 ± 0.24	270
2.	10	14.20 ± 0.20	254
3.	20	14.40 ± 0.30	225
4.	30	14.51 ± 0.21	208
5.	40	14.63 ± 0.21	180
6.	50	14.67 ± 0.17	180

Consequently, increase in the iron filling concentration from 0% to 50% in the probes leads to an enhancement in temperature sensitivity from 14.08 ± 0.24 pm/°C to 14.67 ± 0.17 pm/°C, representing a ∼4.2% improvement in sensitivity.

Figure 5 depicts the variation in temperature sensitivity of the probes with increasing iron filling concentration. It reveals a linear trend in the increase of temperature sensitivity from 0% to 40% iron concentration. However, beyond 40%, the temperature sensitivity only slightly increases from 14.63 ± 0.21 pm/°C to 14.67 ± 0.17 pm/°C, which falls within the measurement uncertainty of the probe with 40% iron concentration.

Response time of a sensor is a key factor in determining performance of the sensor. Response times of the sensing probes are estimated by keeping the probes inside the already heated furnace at 700 °C, and shift in λ_B is recorded with time by using the OSA. For each probe, the experiment is repeated three times and average shift in λ_B is calculated, as shown in Figure 6(a). With increase in iron filling concentration from 0% to 40 %, response time is found to be linearly enhanced from 270 s to 180 s which is 33.3% improvement

in their response times as shown in Figure 6(b). With 50% iron filling concentration, time response is also found to be 180 s. Hence, response time saturates after 40 % iron fillings concentration. The improvement in temperature sensitivities and response times of the sensors is due to better thermal conductivity of iron-ceramic blend structure than the plain ceramic: Table 1 presents temperature sensitivities and temporal response of the sensing probes with iron concentrations varying from 0% to 50%. Observing that the temperature sensitivity and response time of the sensing probes reached saturation after adding 40% iron fillings, we optimized the probe with 40% iron fillings for further analysis.

Ensuring the longevity of a high-temperature sensor is crucial to validate its effective use over an extended period. In order to analyze the sensor's lifespan, the sensing probe containing 40% iron fillings was subjected to a one-hour exposure in a preheated furnace at 700 °C. The variation in reflection power of the FBG was measured using the high-speed power meter. Figure 7 illustrates the changes in optical power of the FBG enclosed within the optimized probe. During the constant annealing process lasting one hour, the optical power of the FBG decreased from 47 µW (92%) to 41 µW (75%). To conduct the lifespan analysis, a method based on the normalized integrated coupling coefficient (NICC) was employed. The NICC value was calculated as part of the analysis as [36]:

$$\eta = \frac{Tanh^{-1}\sqrt{R_t}}{Tanh^{-1}\sqrt{R_o}} \qquad (2)$$

where η represents NICC, R_o is the initial reflected power of the optimized probe which is 92% and R_t is the reflected power of the

Figure 6
(a) Temporal response of FBGs encapsulated in the probes with sudden increase in temperature from 25°C to 700°C. Inset figure represents zoom in view when variation in Bragg wavelength of the FBGs is 90% (b) Variation in heating time response of the probes with increase in iron filling concentration
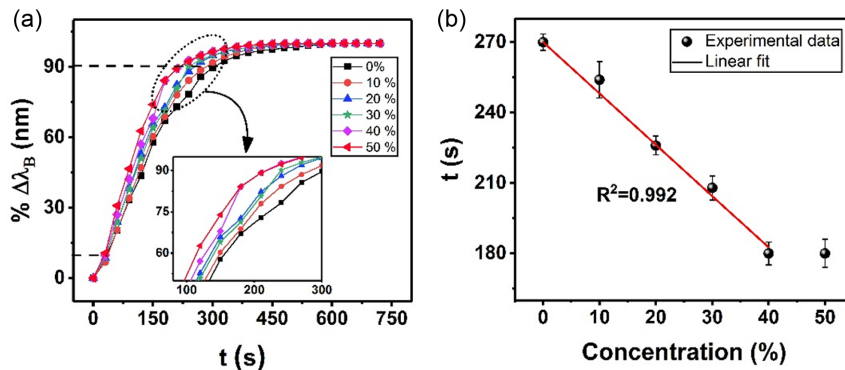
Figure 7
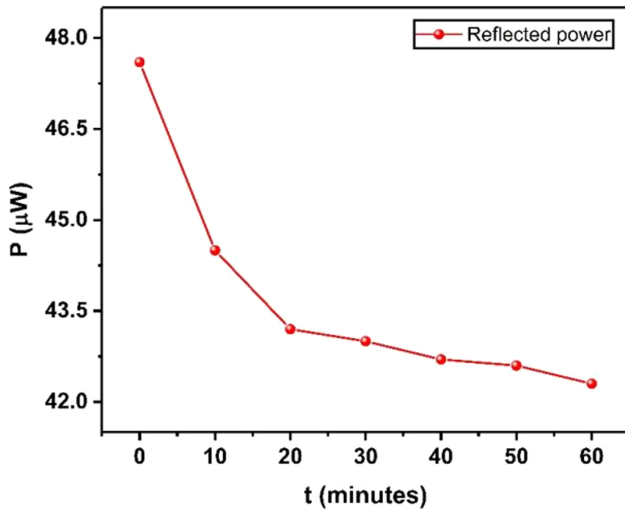**Variation in reflected power of an FBG with time at 700°C temperature**
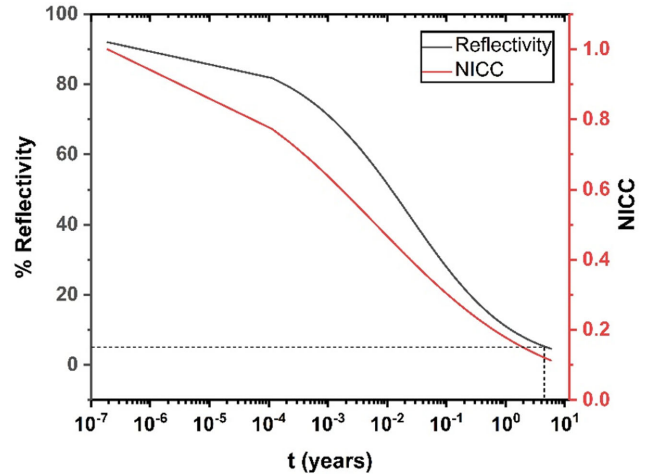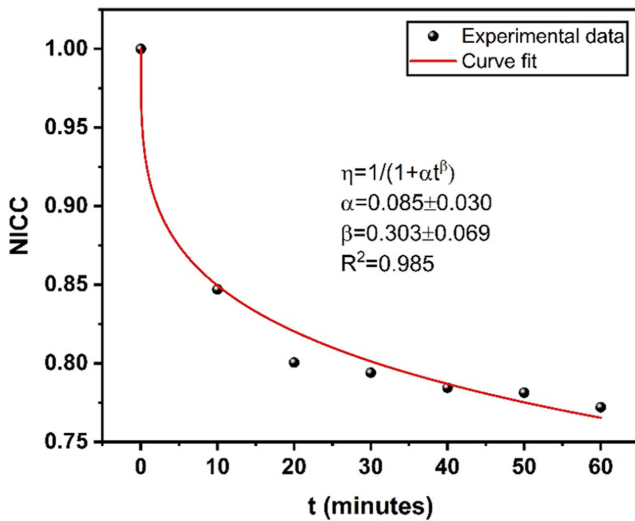

Figure 8
Variation in NICC with time at 700°C temperature where η in the fitted equation represents NICC

probe after time "t" after being constant heating at 700 °C. Variation in NICC with constant heating at 700 °C for 1 hour is shown in Figure 8.

Variation in NICC with time is fitted with power law [36]:

$$\eta = \frac{1}{1 + \alpha(t/t_1)^\beta} \tag{3}$$

where t_1 is time interval of 1 min while α is power law factor and β is power law decay coefficient. From Equation (2) and Equation (3), reflectivity of the probe after time t is:

$$R_t = tanh^2\left(\frac{tanh^{-1}\sqrt{R_o}}{1 + \alpha t^\beta}\right) \tag{4}$$

Figure 9 presents the simulated outcomes for the reflectivity and NICC of the optimized probe. The probe's reflectivity remains at

Figure 9
Simulated variation in reflectivity and NICC of the optimized probe with time

5% even after an estimated lifespan of 4.46 years, with a residual NICC of 12.37%.

In order to investigate any permanent wavelength drift or hysteresis in the FBG enclosed within the sensing probe at high temperatures, the repeatability of the thermal response of the optimized probe is assessed. The results are illustrated in Figure 10, showcasing the behavior during multiple high-temperature cycles.

The repeatability analysis is conducted over three high-temperature cycles. Initially, the probe is heated from room temperature to 700 °C within 80 min. It is then maintained at 700 °C for the subsequent 20 min before being cooled down to 600 °C and kept at that temperature for another 20 min. The second cycle follows the same process as the first one. However, during the third cycle, the probe is maintained at 700 °C for 15 min and then cooled to 450 °C. It can also be observed that the FBG is found to be following the response of the k-type thermocouple of the standard box furnace which certifies

Figure 10
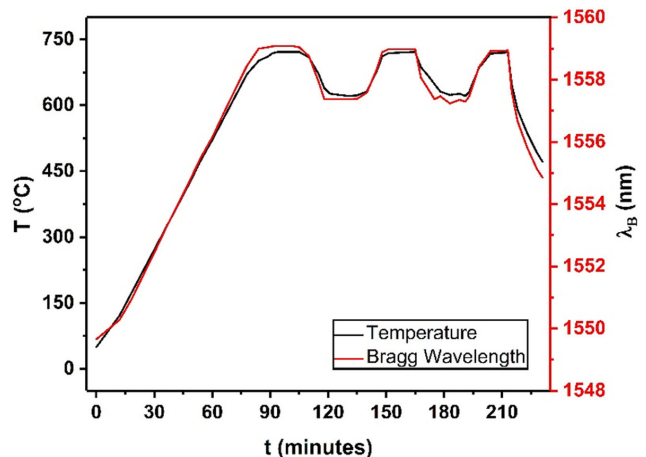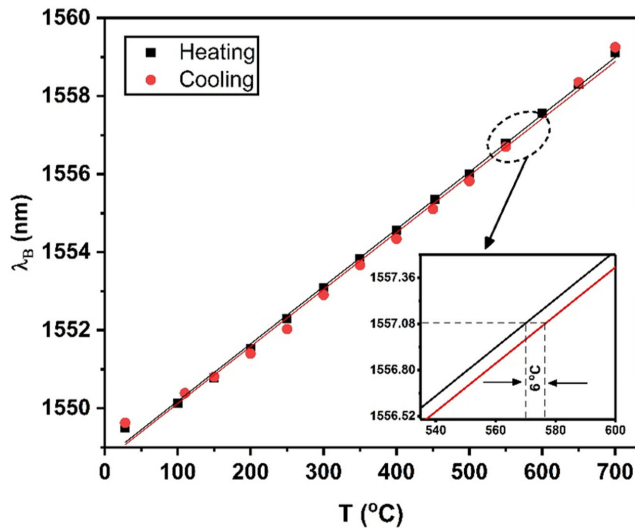**Response of the optimized probe in high-temperature exposure cycles**

Figure 11
Heating and cooling cycle of the optimized probe comprises of heating from room temperature to 700°C and then cooling from 700°C to room temperature. Solid lines represent linear fitting to the experimental data

non-degradation and good repeatability of the optimized probe due to repeated high-temperature exposures. Moreover, there is no permanent drift observed in the wavelength of the encapsulated FBG. The probe shows consistent responses at each point during the thermal cycles, indicating stable and reliable performance even at high temperatures.

The repeatability analysis of the optimized probe is further examined in an additional cycle, where the probe is heated from room temperature to 700 °C and then cooled back from 700 °C to room temperature as shown in Figure 11. During the cooling process, a maximum hysteresis of less than 1% (±6 °C) is observed at certain points. This level of hysteresis is considered negligible for a temperature sensor operating at elevated temperatures. Therefore, the response of the probe in both high-temperature variation cycles and heating-cooling cycle confirms the good repeatability of the probe.

Consequently, the developed probe filled with a mixture of the ceramic and 40% iron fillings was optimized for

high-temperature sensing of type-I FBGs. The optimized probe exhibited thermal stability at elevated temperature 700 °C. Temperature sensitivity, response time, and lifespan of the encapsulated FBG were found to be 14.63 ± 0.21 pm/°C, 180 s response time, and 4.46 years, respectively, and linearity in response exceeding 99%. Comparison of these findings of the optimized probe with earlier studies is listed in Table 2. Additionally, the optimized probe did not exhibit any permanent shift in its λ_B during repeated high-temperature exposure cycles and exhibited less than 1% hysteresis in heat-cooling cycle. This detailed analysis certifies the developed probes filled with mixture of the ceramic and iron fillings for practical robust applications of high-temperature sensing in a harsh environment for an extended period of time.

4. Conclusions

Type-I FBG high-temperature sensors using SS encapsulation and mixture of plain cement ceramic and iron fillings have been developed and experimentally tested for high-temperature sensing up to 700 °C. Six different ceramic-filled sensing probes with 0% to 50% concentrations of iron fillings added to plain concrete blend were developed. The addition of 40% iron fillings resulted in an enhancement of temperature sensitivity, increasing from 14.08 ± 0.24 pm/°C to 14.63 ± 0.21 pm/°C, representing a ∼4.2% improvement in sensitivity with iron fillings. Furthermore, a linear improvement in the response time was observed with iron fillings, reducing it from 270 s to 180 s. This corresponds to a 33.3% improvement in response time as the iron fillings concentration increased from 0% to 40%. However, beyond 40% iron fillings, both temperature sensitivity and response time reached saturation, and probe with 40% iron fillings was optimized for further analyses. The estimated lifespan of the optimized probe, determined using the NICC method, was estimated to be 4.46 years. Importantly, the optimized probe exhibited no permanent drift in its λ_B. The hysteresis observed during a heating-cooling cycle was found to be within ±6 °C, which is less than 1% of the temperature sensing range of the probe. Considering these characteristics, the FBG sensing probe with 40% iron fillings can be confidently recommended for robust, efficient, and reliable high-temperature sensing applications in harsh environments over an extended period of time.

Table 2
Comparison of the optimized developed FBG high-temperature sensor with earlier reported FBG high-temperature sensors

No.	Technique	Maximum temperature (°C)	Sensitivity (pm/°C)	Life-span	Linearity (%)	Reference
1.	RFBG in deuterium-loaded optical fiber	1000	15	500 hours	Non-linear	[37]
2.	RFBG in hydrogen-loaded optical fiber	800	11.95	–	99	[20]
3.	RFBG by post-annealing	1100	16.3	10 min	–	[21]
4.	Packaged RFBG	900	13.72	4 years	Non-linear	[14]
5.	chromium nitride coated FBG	650	14	–	99	[38]
6.	molybdenum-copper coated FBG	800	15.27	1 hour	–	[28]
7.	aluminum nitride encapsulated FBG	500	14.03	–	99	[31]
8.	SS assembly encapsulated FBG	1000	∼2.0[a]	–	Non-linear	[32]
9.	FBG Encapsulation with Ceramic-Iron Synergy	700	14.67	4.46 years	99	Present Work

Note: [a] Calculated from Figure 4 [25], in temperature range 0–800°C

Ethical Statement

This study does not contain any studies with human or animal subjects performed by any of the authors.

Conflicts of Interest

The authors declare that they have no conflicts of interest to this work.

Data Availability Statement

The data that support the findings of this study are available within the manuscript.

Author Contribution Statement

Raja Yasir Mehmood Khan: Conceptualization, Methodology, Software, Validation, Formal analysis, Investigation, Resources, Writing – original draft, Visualization. **Rahim Ullah:** Conceptualization, Validation, Resources, Data curation, Writing – original draft. **Muhammad Faisal:** Conceptualization, Validation, Resources, Data curation, Writing – review & editing, Visualization, Supervision, Project administration.

References

[1] Hsu, C. Y., Chiang, C. C., Hsieh, T. S., Hsu, H. C., Tsai, L., & Hou, C. H. (2021). Study of fiber Bragg gratings with TiN-coated for cryogenic temperature measurement. *Optics & Laser Technology*, *136*, 106768. https://doi.org/10.1016/j.optlastec.2020.106768

[2] Polz, L., Dutz, F. J., Maier, R. R., Bartelt, H., & Roths, J. (2021). Regenerated fibre Bragg gratings: A critical assessment of more than 20 years of investigations. *Optics & Laser Technology*, *134*, 106650. https://doi.org/10.1016/j.optlastec.2020.106650

[3] Khan, R. Y. M., Ullah, R., & Faisal, M. (2023). Design and development of cost-effective fiber Bragg grating temperature sensor package. *Measurement Science and Technology*, *34*(8), 085122. https://doi.org/10.1088/1361-6501/acd01c

[4] Ullah, R., Khan, R. Y. M., & Faisal, M. (2023). Design and development of an economical temperature compensated bidirectional fiber Bragg grating flow sensor. *Engineering Research Express*, *5*(1), 015034. https://doi.org/10.1088/2631-8695/acba69

[5] Grobnic, D., Hnatovsky, C., Dedyulin, S., Walker, R. B., Ding, H., & Mihailov, S. J. (2021). Fiber Bragg grating wavelength drift in long-term high temperature annealing. *Sensors*, *21*(4), 1454. https://doi.org/10.3390/s21041454

[6] Roman, M., Balogun, D., Zhuang, Y., Gerald, R. E., Bartlett, L., O'Malley, R. J., & Huang, J. (2020). A spatially distributed fiber-optic temperature sensor for applications in the steel industry. *Sensors*, *20*(14), 3900. https://doi.org/10.3390/s20143900

[7] Min, R., Liu, Z., Pereira, L., Yang, C., Sui, Q., & Marques, C. (2021). Optical fiber sensing for marine environment and marine structural health monitoring: A review. *Optics & Laser Technology*, *140*, 107082. https://doi.org/10.1016/j.optlastec.2021.107082

[8] Gnyrya, V. S., Tyurin, Y. I., Kashaykin, P. F., Kulsartov, T. V., Kenzhina, I. E., Zaurbekova, Z. A., . . . , & Shaimerdenov, A. A. (2023). A technique for conducting of reactor in-situ tests of optical fibres and FBG-sensors intended for in-vessel applications in thermonuclear facilities. *Fusion Engineering and Design*, *191*, 113787. https://doi.org/10.1016/j.fusengdes.2023.113787

[9] Hegde, G., Asokan, S., & Hegde, G. (2022). Fiber Bragg grating sensors for aerospace applications: A review. *ISSS Journal of Micro and Smart Systems*, *11*(1), 257–275. https://doi.org/10.1007/s41683-022-00101-z

[10] Popov, S. M., Ryakhovskii, D. V., Kolosovskii, A. O., Voloshin, V. V., Vorob'ev, I. L., Isaev, V. A., . . . , & Butov, O. V. (2023). Features of fiber Bragg grating array inscription for sensing applications. *Bulletin of the Lebedev Physics Institute*, *50*, S1464–S1475. https://doi.org/10.3103/S1068335623602376

[11] Zhang, J., Zhou, Y., Sun, P., Du, D., Cui, J., & Zhao, Q. (2023). Investigating key factors for optimizing FBG inscribed by femtosecond laser. *Optics Communications*, *528*, 129049. https://doi.org/10.1016/j.optcom.2022.129049

[12] Li, C., Tang, J., Cheng, C., Cai, L., & Yang, M. (2021). FBG arrays for quasi-distributed sensing: A review. *Photonic Sensors*, *11*, 91–108. https://doi.org/10.1007/s13320-021-0615-8

[13] Cavillon, M., Lancry, M., Poumellec, B., Wang, Y., Canning, J., Cook, K., . . . , & Ballato, J. (2019). Overview of high temperature fibre Bragg gratings and potential improvement using highly doped aluminosilicate glass optical fibres. *Journal of Physics: Photonics*, *1*(4), 042001. https://doi.org/10.1088/2515-7647/ab382f

[14] Kumar, J., Singh, G., Saxena, M. K., Prakash, O., Dixit, S. K., & Nakhe, S. V. (2020). Development and studies on FBG temperature sensor for applications in nuclear fuel cycle facilities. *IEEE Sensors Journal*, *21*(6), 7613–7619. https://doi.org/10.1109/JSEN.2020.3046244

[15] Ma, S., Xu, Y., Pang, Y., Zhao, X., Li, Y., Qin, Z., . . . , & Bao, X. (2022). Optical fiber sensors for high-temperature monitoring: A review. *Sensors*, *22*(15), 5722. https://doi.org/10.3390/s22155722

[16] Afroozeh, A. (2021). Highly sensitive FBG-based sensor for temperature measurement operating in optical fiber. *Plasmonics*, *16*(6), 1973–1982. https://doi.org/10.1007/s11468-021-01457-y

[17] Tian, Q., Xin, G., Lim, K. S., Ee, Y. J., Xue, F., He, Y., . . . , & Yang, H. (2022). Optical fiber sensor with double tubes for accurate strain and temperature measurement under high temperature up to 1000°C. *IEEE Sensors Journal*, *22*(12), 11710–11716. https://doi.org/10.1109/JSEN.2022.3167950

[18] Li, Z., Yu, F., Saito, O., & Okabe, Y. (2023). In-situ laser-ultrasonic visualization with the use of regenerated fiber Bragg grating sensors at elevated temperatures. *Mechanical Systems and Signal Processing*, *188*, 110007. https://doi.org/10.1016/j.ymssp.2022.110007

[19] Bian, Q., Dutz, F. J., Lindner, M., Buchfellner, F., Stadler, A., Jakobi, M., . . . , & Roths, J. (2023). Regenerated fiber Bragg gratings in large mode area fibers for high-temperature sensing. *Journal of Lightwave Technology*, *41*(10), 3175–3181. https://doi.org/10.1109/JLT.2023.3241861

[20] Yu, H., Li, G., Li, X., & Guo, H. (2014). Producing regenerated gratings in hydrogen-loaded single mode fiber by heat treatment. *Photonic Sensors*, *4*, 125–127. https://doi.org/10.1007/s13320-014-0175-2

[21] Wang, T., Shao, L. Y., Canning, J., & Cook, K. (2013). Temperature and strain characterization of regenerated gratings. *Optics Letters*, *38*(3), 247–249. https://doi.org/10.1364/OL.38.000247

[22] Sato, K. A., de Moura, C. C., Ribeiro Filho, A. C., Moreira, L. C., Kalinowski, H. J., Abe, I., & de Oliveira, V. (2022). RFBG thermal aging evaluation above regeneration temperature. *IEEE Sensors Journal*, *22*(19), 18486–18492. https://doi.org/10.1109/JSEN.2022.3199993.

[23] Lupi, C., Vendittozzi, C., Ciro, E., & Felli, F. (2022). FBG spectrum regeneration by Ni-coating and high-temperature

treatment. *Sensors*, *22*(19), 7255. https://doi.org/10.3390/s22197255

[24] Lupi, C., Felli, F., Dell'Era, A., Ciro, E., Caponero, M. A., Kalinowski, H. J., & Vendittozzi, C. (2019). Critical issues of double-metal layer coating on FBG for applications at high temperatures. *Sensors*, *19*(18), 3824. https://doi.org/10.3390/s19183824

[25] Feng, D., Liu, Y., Luo, X., & Zhang, X. (2020). Experimental study on high temperature regeneration of fiber Bragg grating. In *Sixth Symposium on Novel Optoelectronic Detection Technology and Applications*, *11455*, 114555H. https://doi.org/10.1117/12.2565067

[26] Chah, K., Yüksel, K., Kinet, D., Yazd, N. S., Mégret, P., & Caucheteur, C. (2019). Fiber Bragg grating regeneration at 450 °C for improved high temperature sensing. *Optics Letters*, *44*(16), 4036–4039. https://doi.org/10.1364/OL.44.004036

[27] Wang, X., Sun, X., Hu, Y., Zeng, L., Liu, Q., & Duan, J. A. (2022). Highly-sensitive fiber Bragg grating temperature sensors with metallic coatings. *Optik*, *262*, 169337. https://doi.org/10.1016/j.ijleo.2022.169337

[28] He, J., Ding, L., Cai, J., Zhu, W., & Dai, J. (2019). A novel high temperature resistant Mo-Cu functional gradient coating for optic fiber Bragg grating. *Results in Physics*, *14*, 102456. https://doi.org/10.1016/j.rinp.2019.102456

[29] Guo, Y., Xiong, L., & Liu, H. (2019). Research on the durability of metal-packaged fiber Bragg grating sensors. *IEEE Photonics Technology Letters*, *31*(7), 525–528. https://doi.org/10.1109/LPT.2019.2900069

[30] Kuncha, S. P., Chakravarthy, B., Ramachandran, H., & Srinivasan, B. (2008). Distributed high temperature sensing using fiber Bragg gratings. *International Journal of Optomechatronics*, *2*(1), 4–15. https://doi.org/10.1080/15599610801985483

[31] Mamidi, V. R., Kamineni, S., Ravinuthala, L. S. P., Thumu, V., & Pachava, V. R. (2014). Characterization of encapsulating materials for fiber Bragg grating-based temperature sensors. *Fiber and Integrated Optics*, *33*(4), 325–335. https://doi.org/10.1080/01468030.2014.932472

[32] Reddy, V., Srimannarayana, K., Prasad, R. S., Apparao, T. V., & Rao, V. P. (2015). FBG-based novel sensor for high-temperature measurement and its low-cost interrogation. In *Optical Sensors 2015*, *9506*, 95060C. https://doi.org/10.1117/12.2181966

[33] Huang, K., Zhang, X., Lu, D., Xu, N., Gan, Y., & Han, X. (2021). The role of iron tailing powder in ultra-high-strength concrete subjected to elevated temperatures. *Advances in Civil Engineering*, *2021*(1), 6681429. https://doi.org/10.1155/2021/6681429

[34] Dawood, A., Al-Khazraji, H., & Mahmood, D. (2023). Shear behaviour of reinforced-concrete beams incorporating iron filings as sand replacement. *Advances in Civil and Architectural Engineering*, *14*(27), 80–96. https://doi.org/10.13167/2023.27.6

[35] Jain, B., & Sancheti, G. (2023). Influence of silica fume and iron dust on mechanical properties of concrete. *Construction and Building Materials*, *409*, 133910. https://doi.org/10.1016/j.conbuildmat.2023.133910

[36] Erdogan, T., Mizrahi, V., Lemaire, P. J., & Monroe, D. (1994). Decay of ultraviolet-induced fiber Bragg gratings. *Journal of Applied Physics*, *76*(1), 73–80. https://doi.org/10.1063/1.357062

[37] Celikin, M., Barba, D., Bastola, B., Ruediger, A., & Rosei, F. (2016). Development of regenerated fiber Bragg grating sensors with long-term stability. *Optics Express*, *24*(19), 21897–21909. https://doi.org/10.1364/OE.24.021897

[38] Hsiao, T. C., Hsieh, T. S., Chen, Y. C., Huang, S. C., & Chiang, C. C. (2016). Metal-coated fiber Bragg grating for dynamic temperature sensor. *Optik*, *127*(22), 10740–10745. https://doi.org/10.1016/j.ijleo.2016.08.110